Int. J. Electrochem. Sci., 8 **(2013)** 11033 - 11047

International Journal of
ELECTROCHEMICAL
SCIENCE
www.electrochemsci.org

CV and EIS Study of Hydrogen Fuel Cell Durability in Automotive Applications

Fortunato Migliardini, Pasquale Corbo[*]

Istituto Motori, National Research Council of Italy, Via Marconi, 8 - 80125 Naples, Italy
[*]E-mail: p.corbo@im.cnr.it

Received: 31 May 2013 / *Accepted:* 21 June 2013 / *Published:* 20 August 2013

The purpose of this paper was to investigate the main issues of the hydrogen fuel cell durability in relation to a possible application in the transportation sector. The experimental study was effected on a 500W Polymeric Electrolyte Membrane (PEM) stack, previously utilized as a power source in a fuel cell power train for scooter applications. The experimental characterization of the used stack, in terms of polarization curves and individual cell voltage acquisition, evidenced a significant total voltage decrease and a strong irregularity of individual cell voltage. Cyclic Voltammetry (CV) and Electrochemical Impedance Spectroscopy (EIS) were used in order to investigate the possible causes of the stack performance loss. The results evidenced the role of catalyst particles sintering mechanism, associated with the reduction of electrochemical surface area (ECSA) and with the increase of the charge transfer resistance (R_{ct}) observed in the fuel cell electrochemical interface. The possible role of the stack dynamic operation in cell durability was discussed in relation to the hybridization level between fuel cell generator and electric energy storage system.

Keywords: Cyclic Voltammetry; Electrochemical Impedance Spectroscopy; Polymeric Electrolyte Fuel Cell; Fuel Cell Durability, Fuel Cell System Management

1. INTRODUCTION

The most suitable fuel cells for transportation applications use hydrogen as fuel and a polymeric membrane as electrolyte. Besides their low operative temperature (40-80 °C), and then their quick start-up, they are characterized by high power density, high efficiency, good transient response, and absence of corrosive liquid electrolytes, all features strongly appreciated for automotive utilizations [1, 2].

The requirements for fuel cell lifetime vary with the specific application, in particular a duration of at least 5000 h is mandatory for use on cars, while even longer periods are needed for bus and stationary employments (for most applications an acceptable degradation rate is considered to be comprised in the range 2-10 μV/h [3]). However the wide variability of operative conditions usually encountered in automotive applications, such as dynamic driving cycles, startup/shutdown phases and freeze/thaw, make also the target for car very difficult to be met with the current technologies.

Since the concept of durability decay is strictly connected to that of ageing, in the sense of a progressive and not reversible loss of performance, a general examination of this feature for PEM fuel cells has to include some considerations about the main processes that can cause the degradation of materials used for components of these systems (electrocatalysts, membranes and bipolar plates). This degradation is mainly related to working conditions of humidity and temperature, oxidizing or reducing environment, and dynamic operation.

The operation of a fuel cell stack requires the utilization of several auxiliary sub-systems, whose function is to manage reactant feeding, heat and water and to permit an efficient and reliable electric power production [2, 4-7]. The water management is the most critical issue as it is directly connected with the requirement of the electrolytic membrane to be maintained properly humidified. While a strong relationship exists between proton conductivity and water content of Nafion material used as membrane in PEM fuel cell [5], the water produced at cathode side and the air moisture could be not sufficient to maintain properly wet the membranes in all working conditions, because of complex phenomena involving water within the membrane electrode assembly (MEA).

The amount of platinum catalyst used in electrocatalysts of a PEM fuel cell is supported on carbon in the form of nanoparticles, in order to achieve high metal dispersion at relatively low precious metal loading. Then the main problem of ageing of electrocatalysts to be avoided or controlled is the increase of catalyst particle size, which causes diminution of active surface area and then of catalytic activity. The coarsening of Pt nanoparticles during PEM fuel cell operation has been extensively studied, and different mechanisms have been proposed [8-11]. Also corrosion problems of the carbon support have been considered as a cause of electrocatalyst durability loss [12, 13], in particular carbon oxidation can occurr via electrochemical oxidation at the cathode, with formation of CO_2 ($C + 2H_2O = CO_2 + 4H^+ + 4e^-$), or via water gas shift reaction, with production of CO ($C + H_2O = CO + H_2$). Both these routes are catalyzed by Pt and subtract carbon useful for platinum loading, with consequent metal sintering and decrease of the electrochemical surface area [14-19].

Another critical issue regarding durability of PEM fuel cells is the reliability of the electrolytic membrane, which can undergo mechanical, thermal and chemical/electrochemical degradation [20-22], while the degradation of the gas diffusion layer (GDL) is not clearly assessed because of the difficulties in separating the effects from contiguous elements, such as catalysts and bipolar plates. While some decrease of GDL conductivity and hydrophobicity has been associated to loss of PTFE and carbon, due to temperature and electrochemical surface oxidation during fuel cell operation [23], a recent study suggests that hydrophobicity changes of GDL can be considered negligible in 10000 h tests under high humidification [24].

Cyclic voltammetry and electrochemical impedance spectroscopy are useful tools to analyze electric properties of different materials and interface reaction mechanisms, then they can be considered as powerful techniques to investigate processes occurring within an electrochemical system, helping to evidence the performance changes undergone by such systems when used in real applications and to establish hypothesis about the cause of these modifications [25, 26]. In CV technique the potential of a system is swept forth and back between two set voltage limits while the current is acquired. The current peaks observed in the cyclic voltammogram can provide information about the relative rates of reactions in the electrochemical system. The main advantage of EIS with respect to other physical techniques for the investigation of materials is that the former can be applied “in situ”, i.e. a fuel cell can be studied while energy is produced, with hydrogen flowing through anode and air passing through the cathode.

The aim of this article is to analyze the possible causes of the performance loss of a PEM fuel cell stack when it is utilized as a power source in a fuel cell power train. The experimental characterization of a 500 W stack, previously used for more than 500 h as power generator in a scooter power train, was integrated with the results of an investigation effected by cyclic voltammetry and electrochemical impedance spectroscopy.

2. EXPERIMENTAL

The overall scheme of the fuel cell system utilized for CV and EIS experiments is shown in Figure 1. The plant was constituted by the fuel cell stack, the reactant feeding systems, a cooling fan for stack temperature control and a variable resistive load. Hydrogen as fuel and air as oxidant were fed by high pressure cylinders (200 bar) of high purity (>99.5%). Before feeding the stack both reactants were humidified by flowing through Drechsel bubblers filled with de-ionized water at room temperature. A back pressure regulator at the outlet of cathode side and a fuel purge valve at the outlet of anode side permitted the correct management of both reactants during the tests. Two pressure transducers (PT) were also located upstream the stack to monitor anode and cathode pressure, a mass flow rate controller (MFC) was used to set oxidant flow rate, a thermocouple (Tc) was located inside a cooling plat of the stack to verify its operative temperature. Nitrogen fed by high pressure cylinder (200 bar) of high purity (>99.5%) was also used for pipeline purge at the end of each laboratory test, and to feed cathodic side during CV tests.

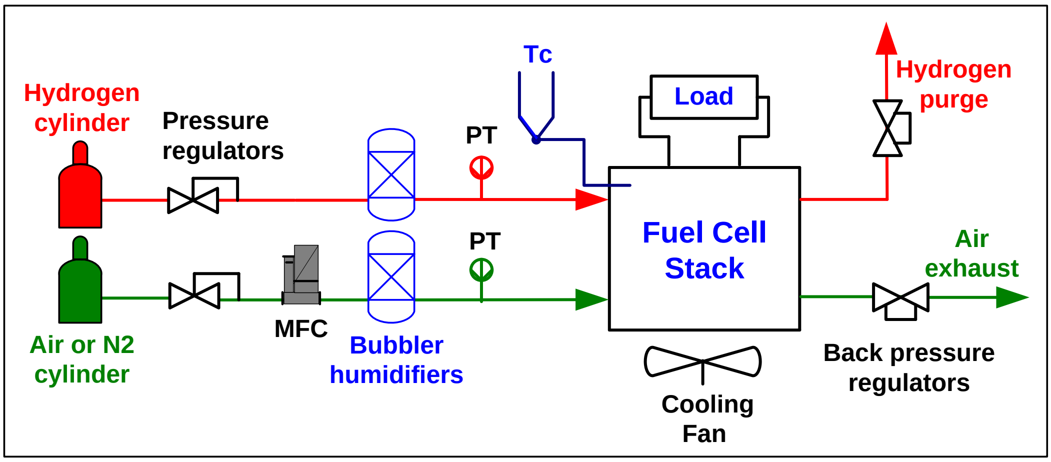

Figure 1. Overall scheme of the fuel cell system utilized in CV and EIS experiments

The stack was constituted by 32 individual elements connected in series and was able to produce a maximum power of 500 W. The main technical specifications are indicated in Table 1. This stack was used for more than 500 h as a power generator in a scooter power train, whose details are reported in a previous work [27], adopting different hybrid configurations characterized by frequent dynamic requirements. CV and EIS analysis were effected on this used stack, after a preliminary characterization in terms of polarization curve and individual cell voltage acquisition.

The cyclic voltammograms were acquired at room temperature and 100 kPa by a Zahner Zennium Electrochemical Workstation coupled with an external Zahner PP201 Potentiostat. The experiments were performed on the 500 W stack feeding anodes with H_2 (0.5 l/min) and cathodes with inert gas (N_2, 0.5 l/min). The electrodes fed by H_2 acted both as counter electrodes and reference electrodes, because of the negligible overpotential at the counter electrode for the hydrogen oxidation, while cathodes acted as working electrodes. The voltage was scanned from 10 to 1200 mV with a sweep rate of 5 mV/s.

Table 1. Technical specifications of the 500 W PEM stack

Specification	Value
Number of cells	32
Active area	64 cm^2
Pt loading	0.4 mg/cm^2
Voltage range	16-30 V
Max power	500 W
Max current	30 A
Max dynamic	100 W/s
Cooling	Forced air

The in situ EIS spectra were acquired in potentiostatic mode by the same Zahner equipment used for CV tests, while the Zahner ZMAN software was used for simulations. The cell part of interest was connected to the potentiostat by a two-electrodes scheme, in which the anode served both as counter electrode and reference electrode. One of most important parameters to be regulated for the execution of a EIS spectrum is the applied frequency (f). At low frequencies (f<1 mHz) the impedance value is mainly affected by the DC conductivity of the electrolyte polymer, while at very high frequencies (f>100 kHz) inductive contributions from connecting wires can appear in the spectrum. Then the range of frequencies used for tests on the 500 W stack was the most significant for fuel cells, comprised between 10 mHz and 10 kHz, where the interfacial properties are evidenced. A potential amplitude of 10 mV was adopted, with points per decades ranging from 5 to 25 in dependence of frequency.

EIS spectra on the used stack were acquired measuring the impedance of different cells at OCV, 40 W and 110 W. In particular the behavior of those cells still adequately performing was comparing to that of cells whose voltage resulted significantly lower as a consequence of aging.

The stack operative conditions were tuned for all tests as follows: T = 298-310 K, stoichiometric ratio = 2.5 at 40 W and 2 at 110 W, p_{air} = 40 kPa, p_{H2} = 40 kPa.

3. RESULTS AND DISCUSSION

3.1. Correlation between hybridization level in a fuel cell power train and stack degradation

The Figure 2 shows the overall scheme of a fuel cell power train with the indication of possible hybrid configurations. The propulsion system comprises the fuel cell generator, the electric energy storage system, a DC-DC converter and the electric drive (composed by inverter and electric machine). The electric parallel between fuel cell generator and electric energy storage system permitted different hybridization levels to be realized, while the DC-DC converter had the function to adequate the stack voltage to the requirements of the electric drive and to regulate the energy flows through the electric bus. In this way the electric power provided by the stack could be directed towards the electric motor or the energy storage system, permitting also regenerative braking to be realized when the electric motor operates as a generator [2,4].

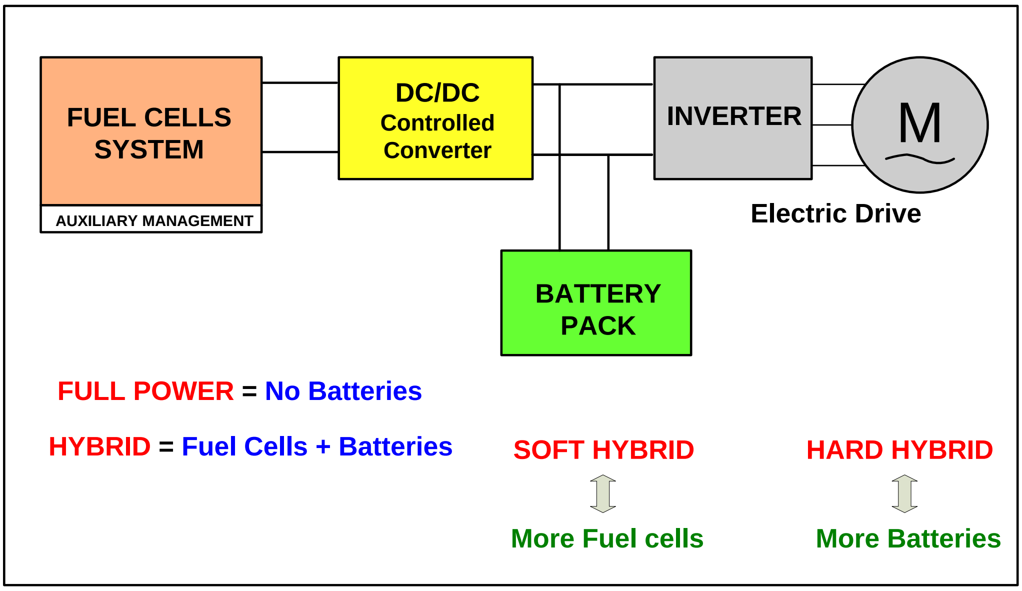

Figure 2. Overall scheme of a fuel cell power train with the indications of possible hybrid configurations

An important qualification for a fuel cell engine in automotive application is its dynamic response to driving requirements. Vehicle drivability require that the power generator is able to deliver maximum power (almost up to 90%) with very short time delay. The fuel cell dynamic operation could involve a partial stack durability reduction, in particular when the fuel cell stack is the only power generator used to feed the electric drive (full power configuration in Figure 2). In this respect the hybridization concept, based on the on-board integration of fuel cell system and electric energy storage devices (traction batteries and/or supercapacitors), would reduce the dynamic requirements to the stack, i.e. electric energy storage systems can assist the fuel cell system during the fast accelerations. Moreover, the presence of storage systems would permit the supplying of vehicle auxiliaries and some energy economy during regenerative braking.

In a soft hybrid configuration the storage system is minimized, and the fuel cell stack generates most of the energy demanded by the load. The load variation requirements have to be satisfied mainly by the fuel cell system, while the storage system could give a limited but useful contribution for satisfying the power requirements during start-up and very fast acceleration phases, damping the high dynamics of the FC generator. In a hard hybrid configuration the role of the storage systems becomes predominant while the power provided by the fuel cell generator is strongly limited, and automotive dynamic requirements are almost completely satisfied by the storage system. The main benefit of the soft hybrid configuration is a minor use of batteries, while the hard hybrid option offers the possibility to use a smaller fuel cell stack, which can work in optimal steady-state conditions. The cost and durability issues related to the fuel cell technology, also together with vehicle type and road mission, could then direct the choice of the hybrid configuration [28, 29].

In Figure 3 the polarization curves of the 500 W stack tested for this paper are reported for the new stack [27] and for the same device after utilization as a power source in a scooter power train in both soft and hard hybrid modalities, while the Figure 4 shows the individual cell voltage acquisition at 110 W.

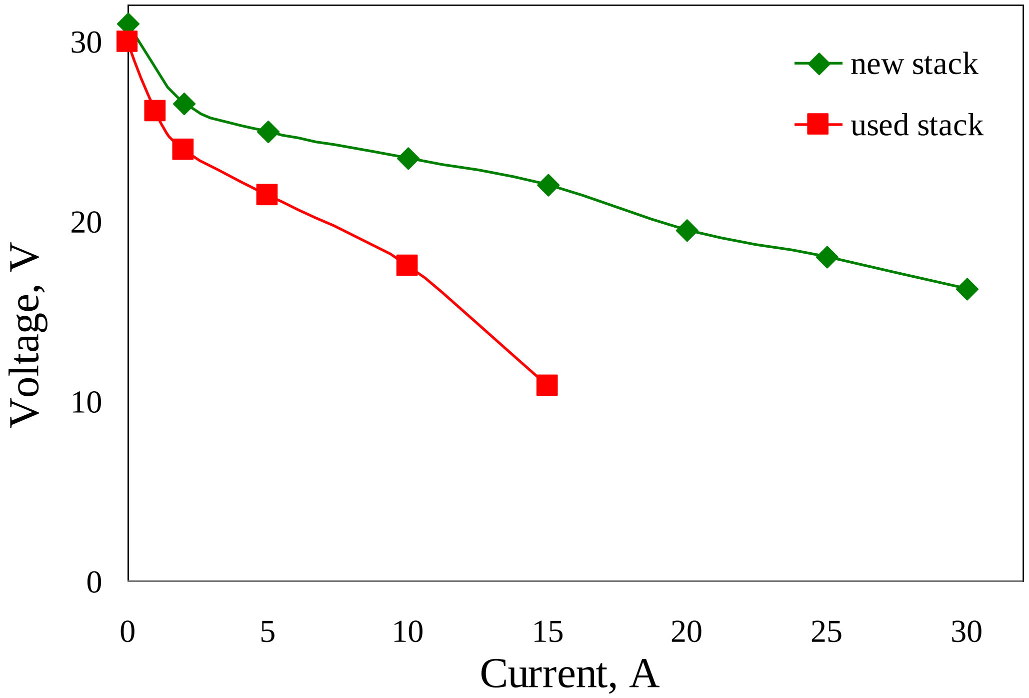

Figure 3. Polarization curves for the 500 W PEM stack before and after utilization in a scooter power train

The results of Figures 3-4 evidence that the utilization of a PEM stack in dynamic conditions, typical of a soft hybrid operation, can determine a performance decrease extended to all cells in terms of cell voltage, but also a worsening of individual cell voltage uniformity. In particular at 15 A the voltage of the used stack resulted 50% lower with respect to the new device (Figure 3). On the other hand data reported in Figure 4, related to a specific acquisition of individual cell voltage (110 W), show a strong irregularity of individual cell voltage. In particular the voltage of the cell N.32 resulted about 0.4 V, while the voltage of the best performing cells was always higher than 0.7 V. Starting from results of Figure 3-4 the used stack was investigated by CV and EIS in order to evidence the durability issues associated with its utilization in a power train, and elucidate the nature of these problems.

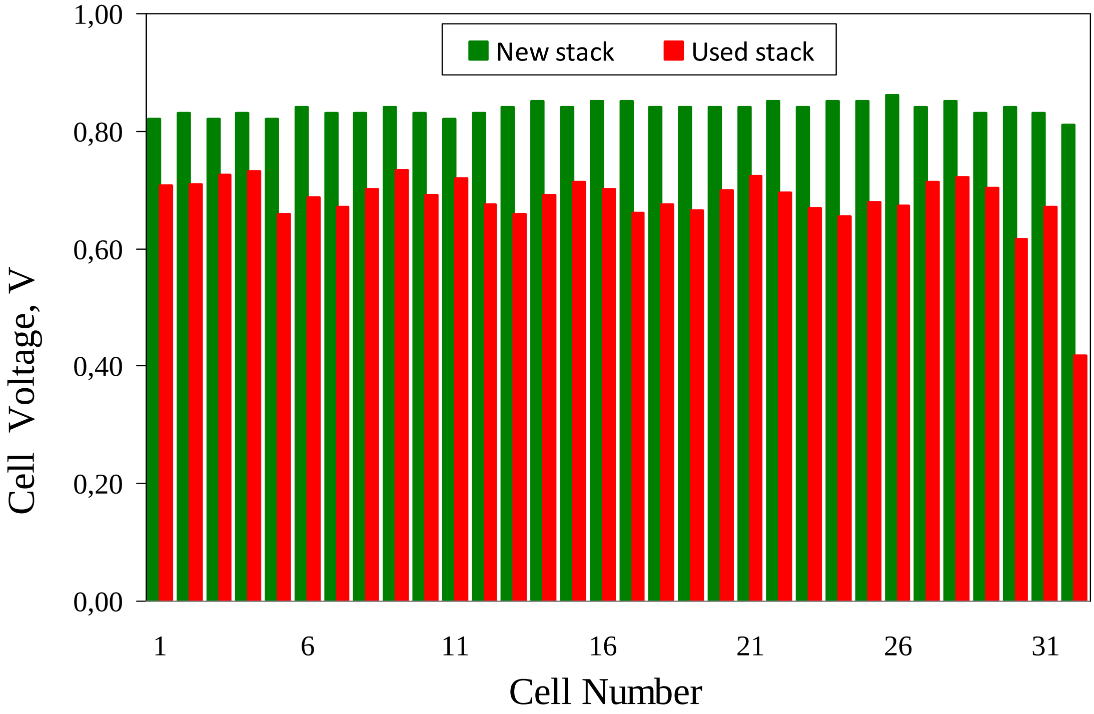

Figure 4. Individual cell voltage acquisition during steady state tests at 110 W on the new and used stack

3.2. Experimental analysis of the fuel cell degradation mechanism by CV and EIS

The characterization by in situ CV was performed on all individual cells of the 500 W stack, in order to obtain a complete information about reactivity conditions of single electrochemical interfaces. In Figure 5 the cyclic voltammograms of one of the best performing cells (cell N.9, on the base of results reported in Figure 4) and of the cell N.32 are shown. The profiles follow the typical trend of Pt surface exposed to H_2 stream [30], in particular a fine structure associated with two hydrogen desorption peaks was detected in the range 0.1÷0.4 V during the anodic sweep of both cells, while the oxidation current peak at 0.6÷0.8 V and the reduction current peak at about 0.9÷1 V were due to the oxidation and reduction of Pt catalyst particles. However the Figure 5 evidences also some important differences between the two cells, in particular the areas of all current peaks before considered are lower for the cell N.32 than for the N.9, and the entire profile is shifted towards higher current values for the cell N.32. While this last phenomenon can be correlated with the presence of some hydrogen crossover [31] the areas under the hydrogen desorption peaks (i.e. the charge associated with the amount of atoms removed from the surface) can be used to have a quantitative indication of the electrochemical surface area (ECSA) of Pt catalyst particles. If the specific charge for a hydrogen monolayer on platinum is assumed equal to 210 $\mu C/cm^2$ of Pt [32, 33], the ECSA can be calculated by the following equation:

$$\text{ECSA } (cm^2{}_{Pt}/g_{Pt}) = \text{charge } (\mu C/cm^2) \,/\, 210\ (\mu C/cm^2{}_{Pt}) \text{ catalyst loading } (g_{Pt}/cm^2)$$

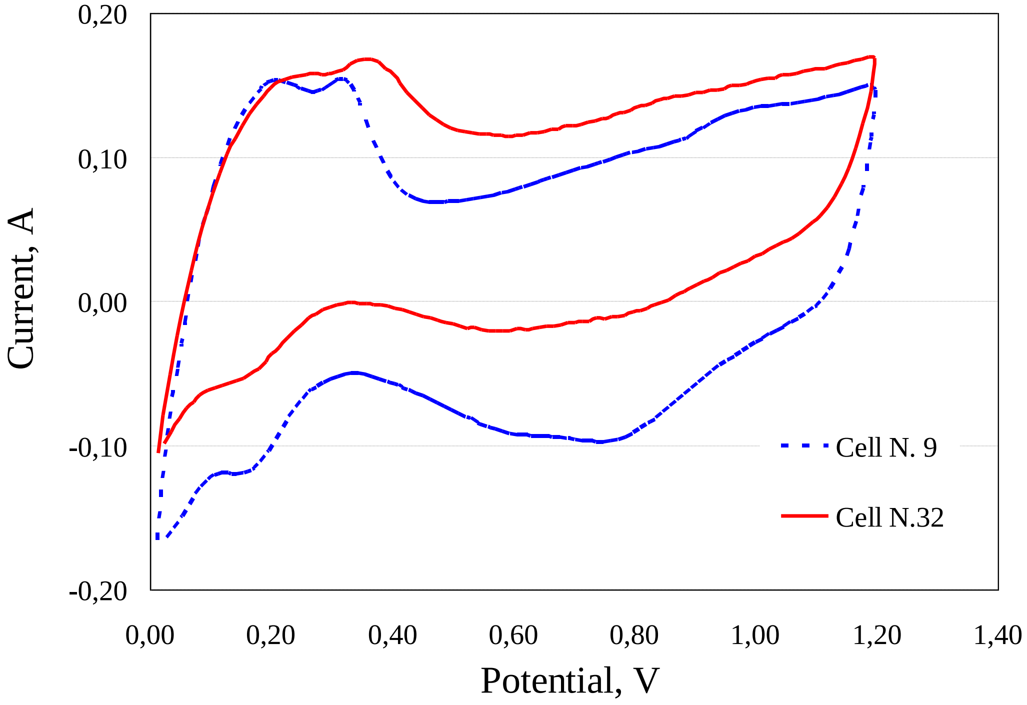

Figure 5. Cyclic voltammetry curves for cells N. 9 and N. 32 of the used 500 W stack

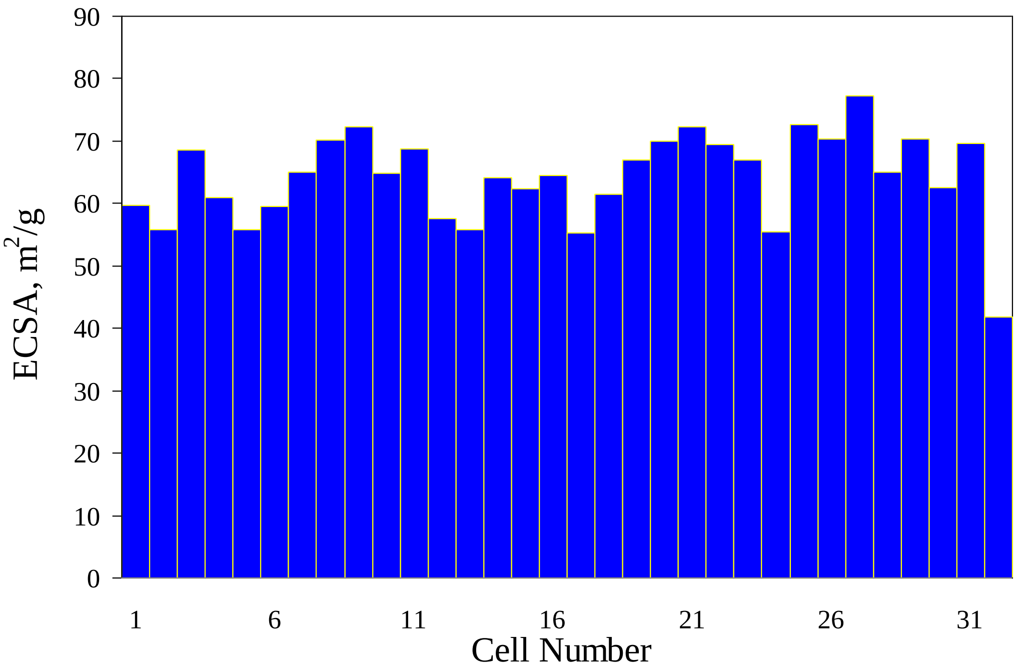

Figure 6. ECSA values for individual cells calculated by CV tests on the used 500 W stack

Using the data reported in Table 1 (64 cm^2 for active area and 0.4 mg/cm^2 for metal loading) the ECSA values were calculated for all individual cells, and reported in the histogram of Figure 6.

The ECSA values can be correlated with the voltage of individual cells reported in Figure 4, in fact the strong irregularity in cell voltage is reproduced in the strong variability of ECSA, whose values ranged from about 40 m^2/g for cell N.32 to almost 80 m^2/g for the best performing cells. This behavior is a clear indication that the agglomeration of catalyst particles has to be considered as a serious cause of the overall decrease in stack performance after ageing, even if CV is not suitable to exclude other possible causes of stack degradation.

The EIS spectra acquired for the cells N.9 and N.32 of the used stack are shown in Figures 7-9, in form of Nyquist plot for different load conditions (OCV, 40 W and 110 W).

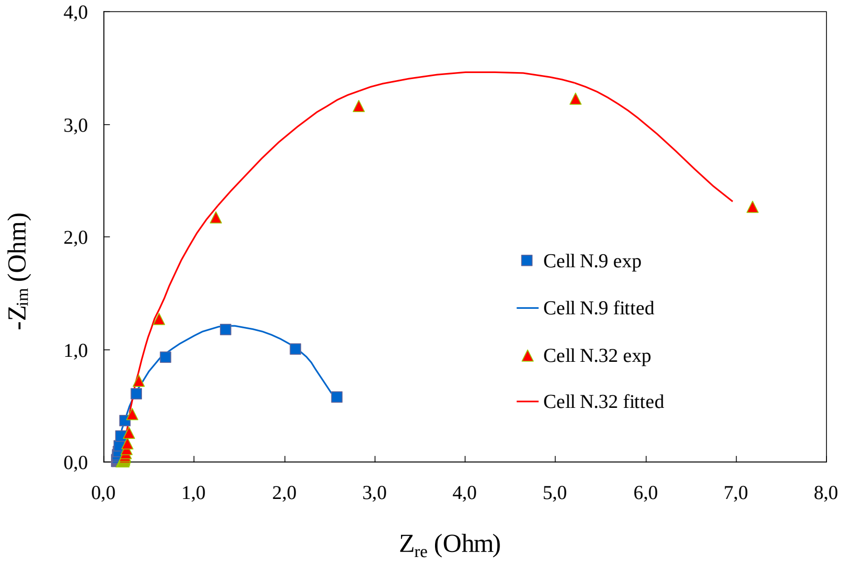

Figure 7. Nyquist plots for N.9 and N.32 cells of the used 500 W stack at OCV. Cell voltage: 0.93 V for N.9 and 0.89 V for N.32. The result of the simulation is indicated by the continuous line.

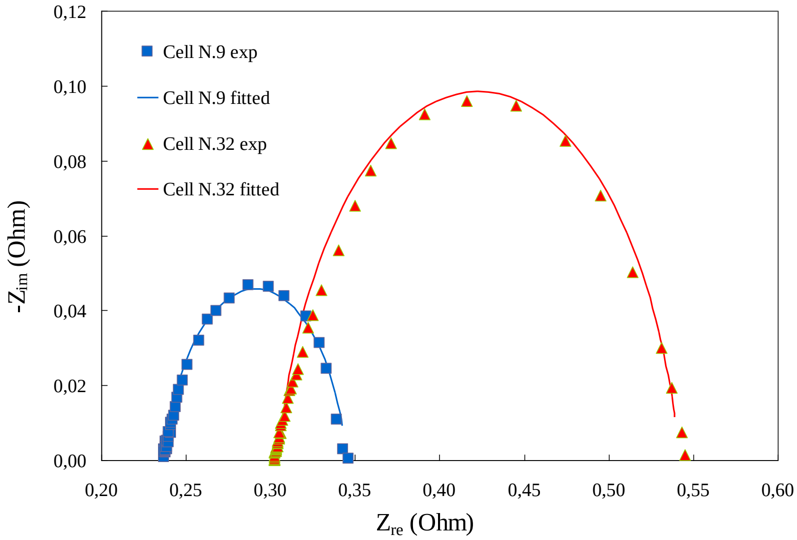

Figure 8. Nyquist plots for N.9 and N.32 cells of the used 500 W stack at 40 W. Cell voltage: 0.84 V for N.9 and 0.75 V for N.32. The result of the simulation is indicated by the continuous line.

All curves are characterized by complete semi-circles typical of a kinetic control associated with the oxygen reduction reaction [34], with significant impedance differences between the two cells and at different load values. In particular the extent of the semicircle resulted higher for the cell N.32 with respect to the N.9 in the three load conditions, showing higher values of both Z_{re} and $-Z_{im}$, while the comparison for the same cell evidenced the effect of the load on $-Z_{im}$ values. These resulted significantly lower (more than one order of magnitude) at 40 and 110 W with respect to OCV, due to the increased rapidity of the electrochemical kinetic. Negative values of $-Z_{im}$ were observed at very high frequencies (not shown in Figures), generally associated with pseudo-inductive features due to the current collector plates plus all metallic components of a single cell [35].

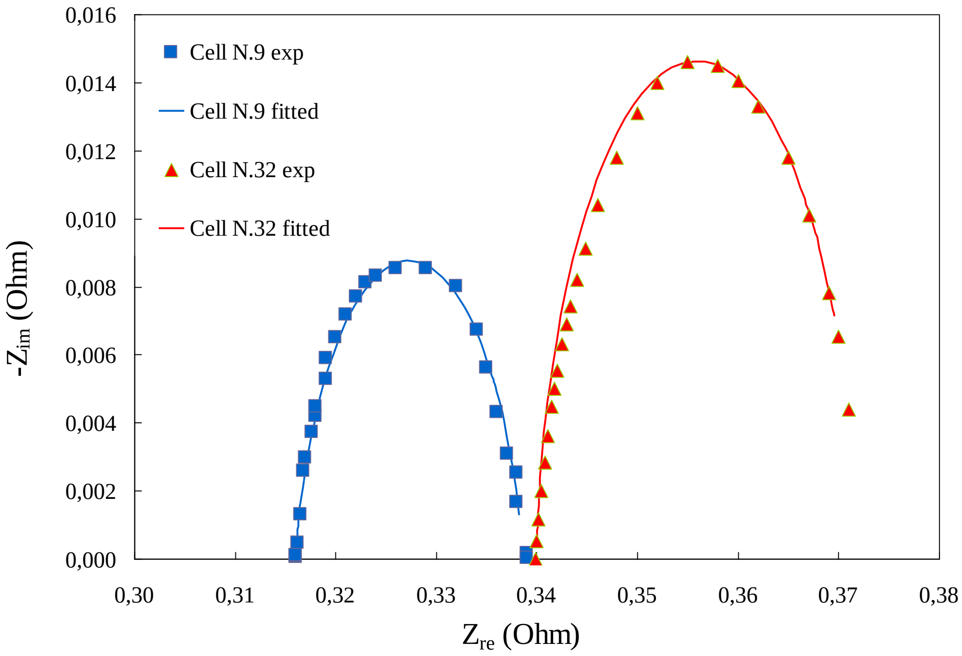

Figure 9. Nyquist plots for N.9 and N.32 cells of the used 500 W stack at 110 W. Cell voltage: 0.73 V for N.9 and 0.42 V for N.32. The result of the simulation is indicated by the continuous line.

EIS experimental data have to be interpreted by the aid of an equivalent electric circuit model. This is a combination of electric and electrochemical elements selected to simulate the response of the electrochemical system to the imposition of the excitation signal. Each element of the model circuit refers to a specific physico-chemical process occurring inside the electrochemical cell, and is responsible of a characteristic impedance behavior. It is known that an electric circuit containing a fuel cell as an active element cannot be approximated to a simple resistor circuit as the real electrochemical systems exhibit more complex behaviors, which are due to the existence of the electrochemical interface. This is generally recognized as the interface between an electronic conductor (electrode) and an ionic conductor (electrolyte). In a fuel cell the ionic resistive behavior is generally assigned to the movement of ions across the electrolyte (proton transport through Nafion membranes), while the most significant electronic resistance in a fuel cell is due to the transfer of electrons at the electrode/electrolyte interface during a redox semi-reaction (charge-transfer resistance, R_{ct}), which depends on the chemical reaction kinetic, the electrode surface and the electrode potential.

In a narrow region of this interface a very thin electric double layer exists, as an important component of the interface. This electrochemical double layer introduces a capacitive contribution (double-layer capacitance, C_{dl}), and can be considered as a plate capacitor created by the pair electrode/electrolyte, where the role of dielectric is performed by the insulating energy barrier present at the interface and due to the transition between ion conduction (within the electrolyte) and electron conduction (within the electrode).

Diffusive phenomena at the interface electrode/electrolyte are essential for the correct operation of a fuel cell, as they are part of the charge transfer reaction, and could give a contribution to the total impedance. The simplest approach to take into account these phenomena would be to introduce the element known as Warburg impedance (Z_W), generally used to describe the mass transport of the electroactive species in layers of infinite thickness [26]. If the electrodic reaction is kinetically favored ($R_{ct} \rightarrow 0$) Z_W is predominant, while for a slow reaction ($R_{ct} \rightarrow \infty$) R_{ct} predominates.

Anode, cathode and electrolyte should be considered as three electric circuits connected in series, however the polymeric membrane is generally treated as a resistor (electrolyte resistance, R_{el}), while being the anode reaction (hydrogen oxidation) very faster than the cathode (oxygen reduction), the electric circuit of the anode can be neglected, and the elements R_{ct}, C_{dl} and W are referred only to the cathode.

On the base of the above considerations, and taking into account that no indication of mass transfer control was observed in EIS spectra, the quantitative analysis of experimental data reported in Figures 7-9 was effected by the equivalent circuit shown in Figure 10, a system constituted by an inductive element connected in series with an ohmic resistance and a RC net [36-38].

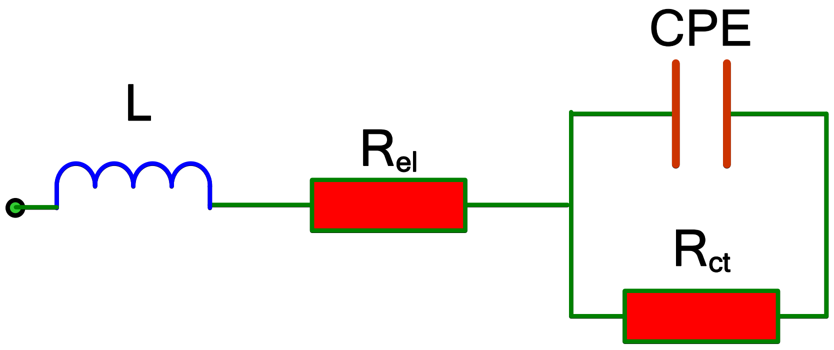

Figure 10. Equivalent circuit used for modelling the data of Figures 7-9

The total ohmic resistance of the stack (R_{el}) is associated with the dominant contribution of the electrolyte membranes, plus ohmic resistances of other cell components (catalyst layer, backing, end plate). In the RC net the charge transfer resistance (R_{ct}), due to the oxygen reduction reaction, is connected in parallel with the double layer capacity, here replaced by a constant phase element (CPE).

A constant phase element is used as a generalized element, directly connected to responses of real systems. The CPE's impedance is given by:

$$Z_{CPE}(\omega) = q^{-1} (i\ \omega)^{-n}$$

where q is a proportionality factor whose physical meaning depends on n value. For integral values of n (n=1, 0, -1) the CPE represents C, R, and L, respectively, while for n=0.5 it gives the Warburg impedance. For any other n value the CPE is associated with the distortions or alterations of behavior of basic elements due to particular conditions of actual systems, such as electrode surface roughness, varying thickness or composition, non-homogeneous reaction rates on the electrode surface. The assumption to use a CPE is justified by the consideration that the double layer capacity is distributed through the porous electrodes of a PEM fuel cell [26].

The fitting was effected by the Levenberg-Marquardt algorithm, and the results are shown by continuous lines in Figures 7-9. The values of the electrochemical parameters obtained by this fitting procedure are reported in Table 2.

Table 2. Fitting electrochemical parameters obtained from EIS spectra of N.9 and N.32 cells by the equivalent circuit of Figure 10.

Cell (Load)	R_{el} (Ω)	R_{ct} (Ω)	q_{CPE} ($\Omega^{-1}s^{n}$)	n_{CPE}
N.9 (OCV)	0.16	2.6	3.2	0.96
N.9 (40 W)	0.24	0.11	3.9	0.91
N.9 (110 W)	0.32	0.023	2.9	0.84
N.32 (OCV)	0.22	7.8	2.7	0.93
N.32 (40 W)	0.31	0.24	1.6	0.88
N.32 (110 W)	0.34	0.032	1.4	0.94

Regarding the values of the ohmic resistance (R_{el}) not negligible differences were observed varying the stack power and between the two cells, however this parameter is associated with the building characteristics of cells and can be strongly affected by the membrane water content, then it does not reflect the stack aging significantly, and it is not useful to explain the voltage differences observed between N.9 and N.32 cells (Figure 4 for 110 W). Instead, the R_{ct} values reported in Table 2 not only evidence the rapid and expectable decrease of the charge transfer resistance with load [35,39,40], but the values of this type of resistance resulted significantly higher for the most aged cell (N.32), indicating a loss of catalytic activity of the electro-catalyst involved in the oxygen reduction reaction.

With regard to CPE parameters the n values were always close to 1, indicating that a capacitive contribution was prevalent in this element, then q values represent with good approximation the behavior of the double layer capacity. The Table 2 shows that the C_{dl} (q) value was about 3 F (for n=1) at OCV for both cells, but resulted lower for the N.32 cell at the highest loads (a diminution of about 50% was observed for this cell passing from OCV to 110 W). These data are compatible with a lower capacitor charging associated with a reduced charge transfer reaction rate. In fact, if the supported catalyst is uniformly distributed over the MEA surface, it is reasonable to assume a direct proportionality between C_{dl} and ECSA [41].

The 500 W stack used for CV and EIS tests reported in the present paper was previously utilized as power source in a hybrid fuel cell power train for scooter application. Because of this type of utilization the stack was undergone to both steady state and dynamic operative conditions, in dependence of the selected hybrid configuration. The characterization results before described can be correlated with three possible phenomena involved during the dynamic stack operation: i) electrode material degradation due to potential cycling; ii) not optimal variation of temperature and humidification conditions; iii) polarity reversal.

For fuel cells fed with pure hydrogen as a fuel, the anode potential remains close to the reversible hydrogen potential, due to the high kinetic of the oxidation reaction, then all load variations are experienced by the cathode. The fast and iterated potential cycling can be correlated with material degradation and consequent alteration of catalyst layer performance, in particular with changes of Pt and carbon oxide coverage, and consequent R_{ct} increase [42].

A frequent transient situation occurring during dynamic operation is characterized by low load and high temperature, the later deriving by a previous utilization at higher loads. In this condition water production in the MEA is scarce, and the water coming from external humidification can rapidly evaporate. The effect of these phenomena consists in a not sufficient membrane hydration, with consequent overall dimensional change, detrimental to its mechanical stability. This process can generate pinholes which result in crossover of reactant gases into their respective reverse electrodes. When this happens, the exothermic hydrogen combustion produces local hot spots on the catalyst surface, which can determine corrosion of carbon support beneath the platinum particles, with consequent catalyst sintering (migration and accumulation) and loss of catalytic activity [43-44]. These phenomena justify the irregularity observed for cell voltage and ECSA, and the difference between R_{ct} values of N.9 and N.32 cells.

The particular performance worsening observed on cell N.32 can be attributed to some hydrogen starvation, more evident for the farthest cell from hydrogen entry and at higher load, which can be the cause of polarity reversal [45].

4. CONCLUSIONS

The experimental study effected in this paper has been focused on the examination of possible aging mechanisms occurring in a PEM fuel cell stack undergone to dynamic operative conditions typical of an automotive application. After 500 h of testing in a scooter power train the 500 W stack showed an significant efficiency loss accompanied by a strong irregularity of individual cell voltages. CV analysis evidenced a strong irregularity of ECSA values for the individual cells of the used stack, which reproduced the poor cell voltage uniformity observed on the used stack under load. The role of catalyst degradation in performance loss was confirmed by EIS, which showed a clear increase of the charge transfer resistance for the most aged cell (N.32).

The catalyst degradation, suggested by both CV and EIS, was associated with the cathode potential cycling, with corrosion phenomena involving both Pt and carbon support, and with the critical conditions of membrane hydration occurring in dynamic working of a fuel cell power train, with local hot spot production and consequent catalyst particles sintering.

A particular performance worsening was observed for the cell N.32, which was the farthest from hydrogen entry. The voltage of this cell resulted about 50% lower with respect to the best performing cells, indicating a more significant degradation of the electrolyte-catalyst interface. This was confirmed by ECSA values, which resulted about 50% lower than those obtained for central cells, and by the significant increase of R_{ct}. The possible role of hydrogen starvation and consequent polarity reversal has been proposed as an additional motivation to explain the strong performance loss of this cell.

The overall results presented in this paper suggest that the utilization of a hard hybrid configuration in a fuel cell vehicle, characterized by a steady state utilization of the stack, could assure a higher reliability of PEM fuel cells.

ACKNOWLEDGMENTS
The authors gratefully acknowledge the Italian Ministry of University and Research for financial support (RITMARE Flagship Project 2012-2016).

References

1. G. Weaver, *World Fuel Cells – An Industry Profile with Market Prospect to 2010,* Elsevier Advanced Technology, Kidlington, Oxford (2002)
2. J. Larminie and A. Dicks, *Fuel Cell Systems Explained*, John Wiley & Sons Ltd, Chichester (2000)
3. S.D. Knights, K.M. Colbow, J. St-Pierre and D.P. Wilkinson, *J Power Sources*, 127 (2004) 127
4. P. Corbo, F. Migliardini and O.Veneri, *Hydrogen Fuel Cells for Road Vehicles*, Springer-Verlag, London (2011)
5. M. Ciureanu, *J Appl Electrochem*, 34 (2004) 705
6. Y. H. Park and J. A. Caton, *J Power Sources*, 179 (2008) 584
7. G. Karimi, F. Jafarpour and X. Li, *J Power Sources*, 187 (2009) 156
8. Y. Shao, G. Yin and Y. Gao, *J Power Sources*, 171 (2007) 558
9. M. Watanabe, K. Tsurumi, T. Mizukami, T. Nakamura and P. Stonehart, *J Electrochem Soc*, 141 (1994) 2659
10. T. Akita, A. Taniguchi, J. Maekawa, Z. Siroma, K. Tanaka, M. Kohyama and K. Yasuda, *J Power Sources,* 159 (2006) 461
11. Y. Zhai, H. Zhang, D. Xing and Z. Shao, *J Power Sources*, 164 (2007) 126
12. S. Maass, F. Finsterwalder, G. Frank, R. Hartmann and C. Merten, *J Power Sources*, 176 (2008) 444
13. H. S. Oh, K. H. Lim, B. Roh, I. Hwang and H. Kim, *Electrochim Acta*, 54 (2009) 6515
14. W. Li and A. M. Lane, *Electrochem Commun*, 11 (2009) 1187
15. D. A. Stevens, M. T. Hicks, G. M. Haugen and J.R. Dahn, *J Electrochem Soc*, 152 (2005) A2309
16. Y. Y. Shao, G. P. Yin, Y. Z. Gao and P.F. Shi, *J Electrochem Soc*, 153 (2006) A1093
17. H. R. Colon-Mercado and B. N. Popov, *J Power Sources*, 155 (2006) 253
18. S. Zhang, X. Z. Yuan, J. N. Cheng Hin and H. Wang, *J Power Sources*, 194 (2009) 588
19. F. Charreteur, F. Jaouen and J. P. Dodelet, *Electrochim Acta*, 54 (2009) 6622

20. A. Collier, H. Wang, X. Yuan, J. Zhang and D. P. Wilkinson, *Int J Hydrogen Energ*, 31 (2006) 1838
21. N. Ramaswamy, N. Hakim, S. Mukerjiee, *Electrochim Acta*, 53 (2008) 3279
22. D. E. Curtin, R. D. Lousenberg, T. J. Henry, P. C. Tangeman and M. E. Tisack, *J Power Sources*, 131 (2004) 41
23. K. H. Kangasniemi, D. A. Condit, T. D. Jarvi, *J Electrochem Soc*, 151 (2004) E125
24. Y. Hiramitsu, H. Sato, H. Hosomi, Y. Aoki, T. Harada, Y. Sakiyama, Y. Nakagawa, K. Kobayashi and M. Hori, *J Power Sources*, 195 (2009) 435
25. J. Wu, X.Z. Yuan, H. Wang, M. Blanco, J.J. Martin, J. Zhang, *Int J Hydrogen Energ*, 33 (2008*)* 1735
26. X. Zi Yuan, C. Song, H. Wangand and J. Zhang, *Electrochemical Impedance Spetroscopy in PEM fuel cells*, Springer-Verlag, London (2010)
27. P. Corbo, F. E. Corcione, F. Migliardini and O. Veneri, *Energy Convers Manage*, 47 (2006) 3255
28. P. Corbo, F. Migliardini and O. Veneri, *Energ Convers Manage*, 49 (2008) 2688
29. P. Corbo, F. Migliardini and O. Veneri, *J Power Sources*, 157 (2006) 799
30. U. Koponen, H. Kumpulainen, M. bergelin, J. Keskinen, T. Peltonen, M. Valkiainen, M. Wasberg, *J Power Sources*, 118 (2003) 325
31. M. Liu, C. wang, F. Xie, Z. Mao, *Int J Hydrogen Energ*, http://dx.doi.org/10.1016/j.ijhydene.2013.02.086
32. B. Li, R. Lin, D. Yang, J. Ma, *Int J Hydrogen Energ*, 35 (2010) 2814
33. X. Wang, I-M. Hsing, P.L. Yue, *J Power Sources*, 96 (2001) 282
34. X. Yuan, H. Wang, J.C. sun, J. Zhang, *Int J Hydrogen Energ*, 32 (2007) 4365
35. S. Asghari, A. Mokmeli and M.Samavati, *Int J Hydrogen Energ*, 35 (2010) 9283
36. C. Brunetto, A. Moschetto and G. Tina, *Electr Pow Syst Res*, 79 (2009) 17
37. M. Kumagai, S. T. Myung, T. Ichikawa and H. Yashiro, *J Power Sources*, 159 (2010) 5501
38. X. Yan, M. Hou, L. Sun, D. Liang, Q. Shen, H. Xu, P. Ming and B.Yi, *Int J Hydrogen Energ*, 32 (2007) 4358
39. T. Romero-Castanon, L. G. Arriaga, U. Cano-Castillo, *J Power Sources*, 118 (2003) 179
40. X. Yuan, J. C. Sun, M. Blanco, H. Wang, J. Zhang, D. P. Wilkinson, *J Power Sources*, 161 (2006) 920
41. J-R. Kim, J.S. Yi, T-W. Song, *J Power Sources*, 220 (2012) 54
42. R. Borup, J. Meyers, B. Pivovar, Y.S. Kim, R. Mukundan, N. Garland, D. Myers, M. Wilson, F. Garzon, D. Wood, P. Zelenay, K. More, K. Stroh, T. Zawodzinski, J. Boncella, J.E. McGrath, M. Inaba, K. Miyatake, M. Hori, K. Ota, Z. Ogumi, S. Miyata, A. Nishikata, Z. Siroma, Y. Uchimoto, K. Yasuda, K. Kimijima, N. Iwashita, *Chem. Rev*. 107 (2007) 3904
43. D. Liu and S. Case, *J Power Sources*, 162 (2006) 521
44. J. Wu, X. Zi Yuan, J. J. Martin, H. Wang, J. Zhang, J. Shen, S. Wu, W. Merida, *J Power Sources*, 184 (2008) 104
45. M.A. Travassos, V.V. Lopes, R.A. Silva, A.Q. Novais, C.M. Rangel, *Int J Hydrogen Energ*, http://dx.doi.org/10.1016/j.ijhydene.2013.01.132